Venus Climate Database v2.3
Validation Document

S. Lebonnois, E. Millour, F. Forget, A. Martinez, A. Boissinot, T. Pierron
Laboratoire de Météorologie Dynamique, IPSL, Paris, France

May 2023

Abstract

This document details the validation of the Venus Climate Database (VCD) software. First, it validates some features included in the VCD: the interpolation between EUV flux scenarios, the rebuilding of variability based on EOF decomposition, and small-scale gravity waves. Second, a systematic comparison is done against all available observational datasets, in order to document the ability of the VCD to predict the atmospheric state, as well as its possible biases.

Contents

List of acronyms

- DDD: Detailed Design Document
- EOF: Empirical Orthogonal Functions
- IPSL Venus GCM: Venus Global Climate Model of the Pierre-Simon Laplace Institute
- VCD: Venus Climate Database
- VenusGRAM: Venus Global Reference Atmospheric Model
- VIRA: Venus International Reference Atmosphere

1 Validation of Venus Climate Database features

1.1 EUV scenarios 4 and 5: interpolation of the EUV input flux

To build the VCD, the IPSL Venus GCM was run using three different EUV input fluxes, based on the E10.7 index. The values fixed for E10.7 were: 70 s.f.u. (EUV minimum, scenario 2), 140 s.f.u. (average EUV, scenario 1) and 300 s.f.u. (EUV maximum, scenario 3).

However, the VCD offers the possibility to choose a different value for the E10.7 index, with EUV scenario 4 where the E10.7 index is chosen as the observed value at a given terrestrial date, and EUV scenario 5 where the E10.7 index is chosen directly by the user. For these scenarios, atmospheric variables are linearly interpolated between two of the VCD files obtained from GCM simulations.

To validate this interpolation, additional GCM simulations were done at E10.7=100 and 200 s.f.u., with 5 Venus days of simulations. The fields were averaged over the duration of the simulation, like it is done for VCD files. We compared in Figs. 1, 2 and 3 some variables from these two simulations (temperature, density and winds) with the variables obtained from the VCD EUV scenario 5, for the three different albedo scenarios.

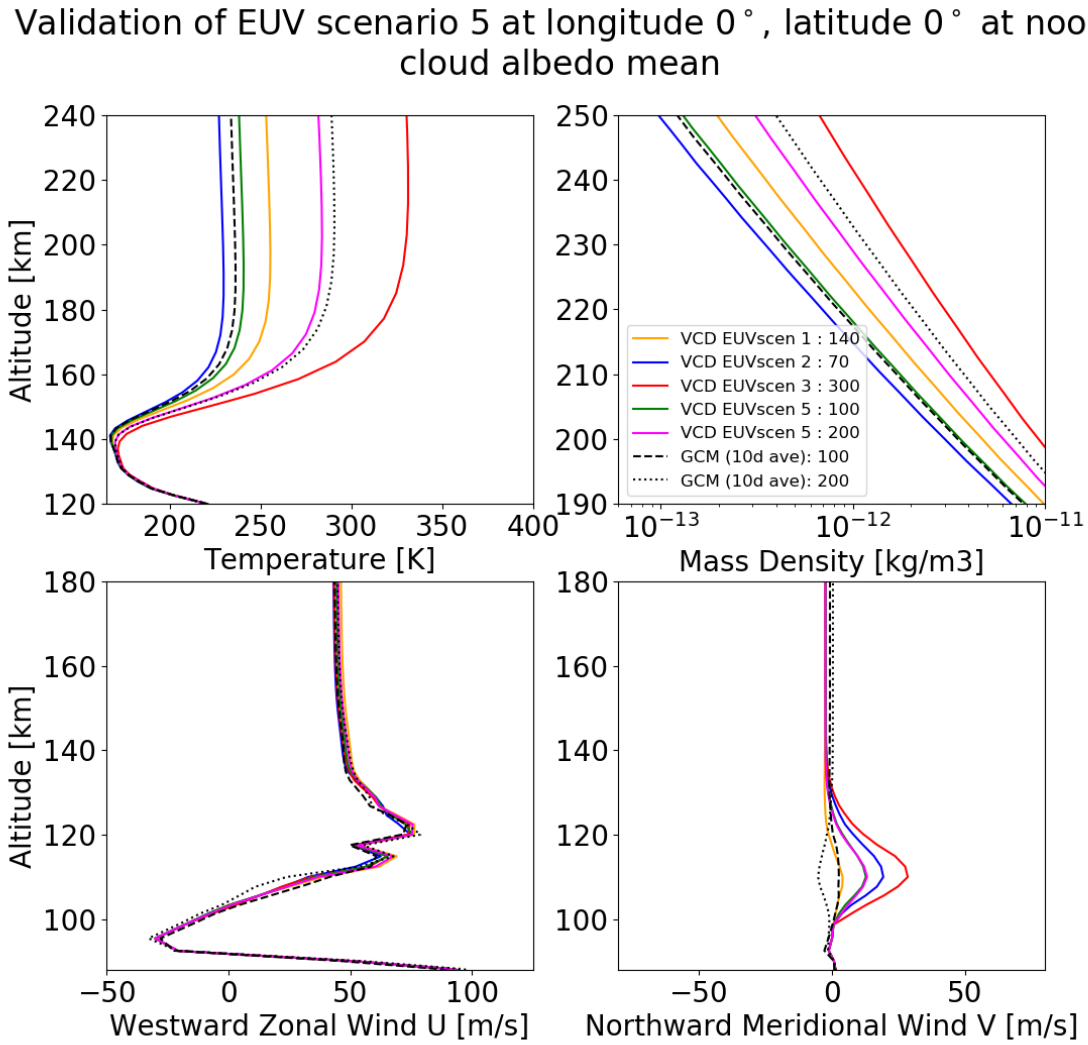

Figure 1: Comparisons between GCM simulations at E10.7=100 and 200 s.f.u. and VCD EUV scenario 5 for the same E10.7 values, for vertical profiles of temperature, density, and horizontal winds at longitude 0°, latitude 0° and local time 12h. Albedo scenario is standard.

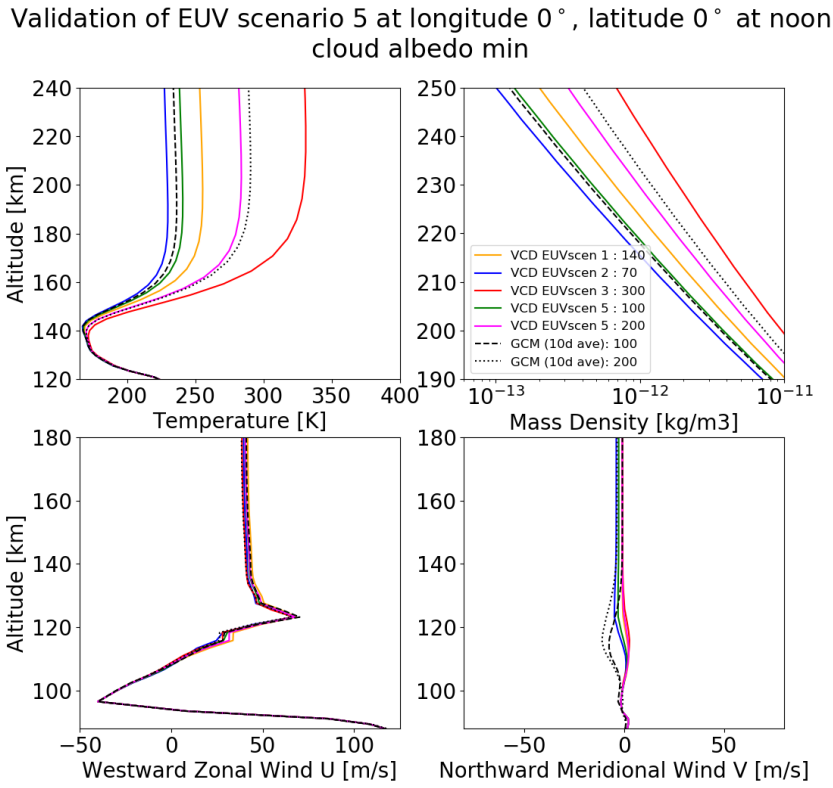

Figure 2: Same as Fig. 1, but for the low albedo scenario.

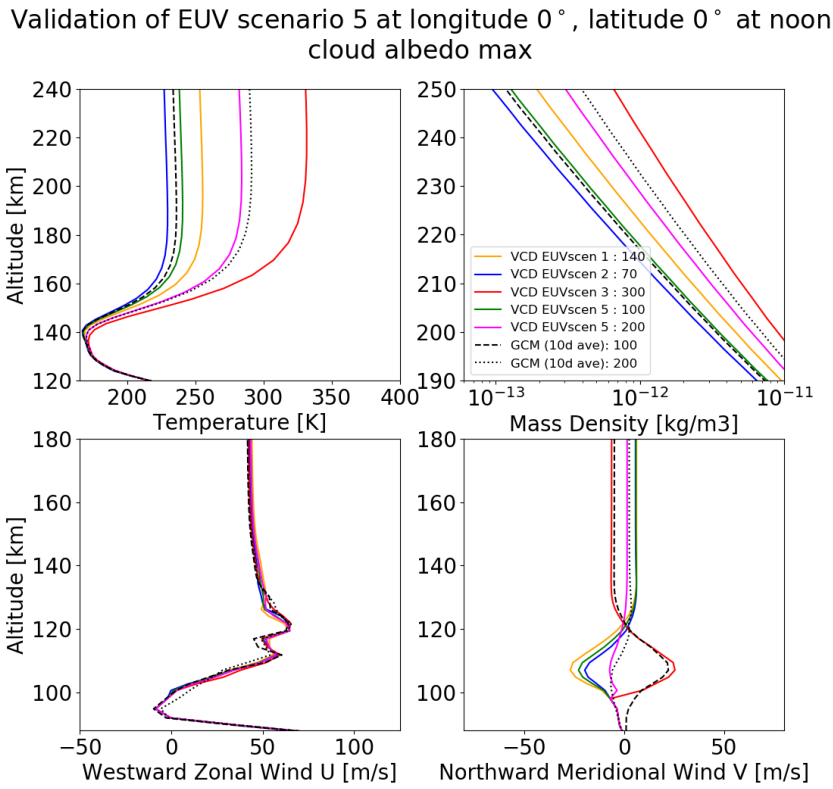

Figure 3: Same as Fig. 1, but for the high albedo scenario.

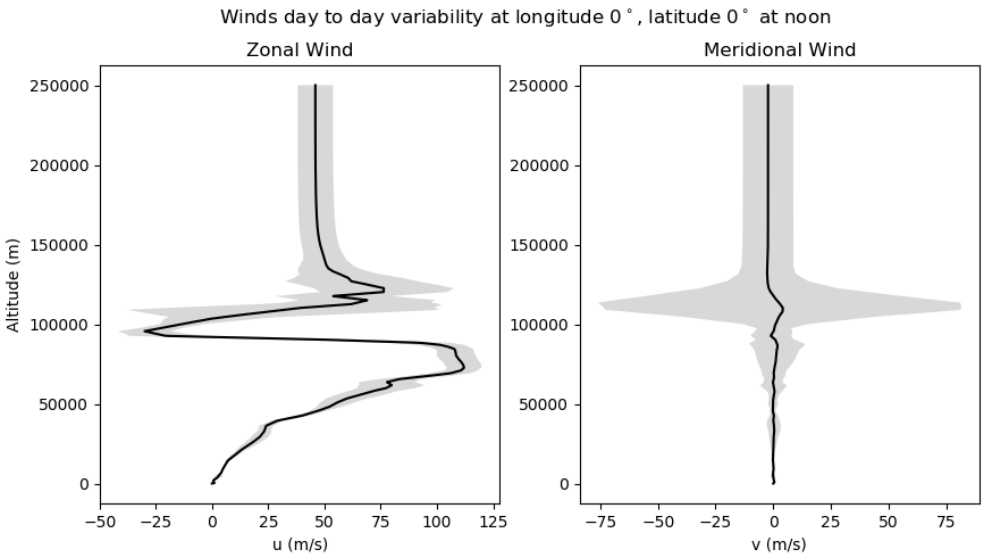

Figure 4: Zonal and meridional wind variability (Day-to-day) at longitude 0°, latitude 0° and local time 12h. Albedo scenario is standard, figures for the other albedo scenarios are similar.

For temperature and density, linear interpolation produces satisfying results, with temperature errors up to 7K in the exosphere at noon, and density relative errors up to 15%. For winds, variability is large, both within one LT hour and from day to day, as shown in Fig. 4, which explains the discrepancies. Moreover, note that VCD files correspond to climatological days, which are made from averaging 10 days of simulation whereas the GCM simulations are averaged on only 5 days.

1.2 Reconstructing the variability from EOFs

The VCD includes the average climatology of the atmospheric fields, as well as their variability. A perturbed state can be obtained when including large-scale perturbations, based on an EOF decomposition of the atmosphere. The goal of this section is to validate this EOF decomposition through a comparison between its variability, and the recorded one (hourly variability, see DDD).

It was chosen to retain a number of EOFs of 200 to be able to reconstruct as best as possible the meteorology. In order to check that this number was sufficient we compared the hourly RMS of the VCD with a recalculated one from 50 days simulated with the VCD using the large scale perturbation mode. This comparison is done on Fig. 5 at several altitudes: 50 km, 100 km and 150 km. The comparison was made for the temperature, the zonal wind, the surface pressure and the density, the latest being deduced from the perturbed temperature vertical profile and the perturbed surface pressure. The comparison gives broadly similar RMS. The comparison was done on other points on the planet where the results are quite similar to what was obtained on Fig. 5.

The agreement could be further improved by computing several EOFs data files for different GCM days so that, for a given date, an extra variability could be taken into account via a randomization of the data file used by the VCD. Eventually, a realistic simulation of the atmospheric variability includes necessarily the small scale perturbations induced by the gravity waves as an important source of variability.

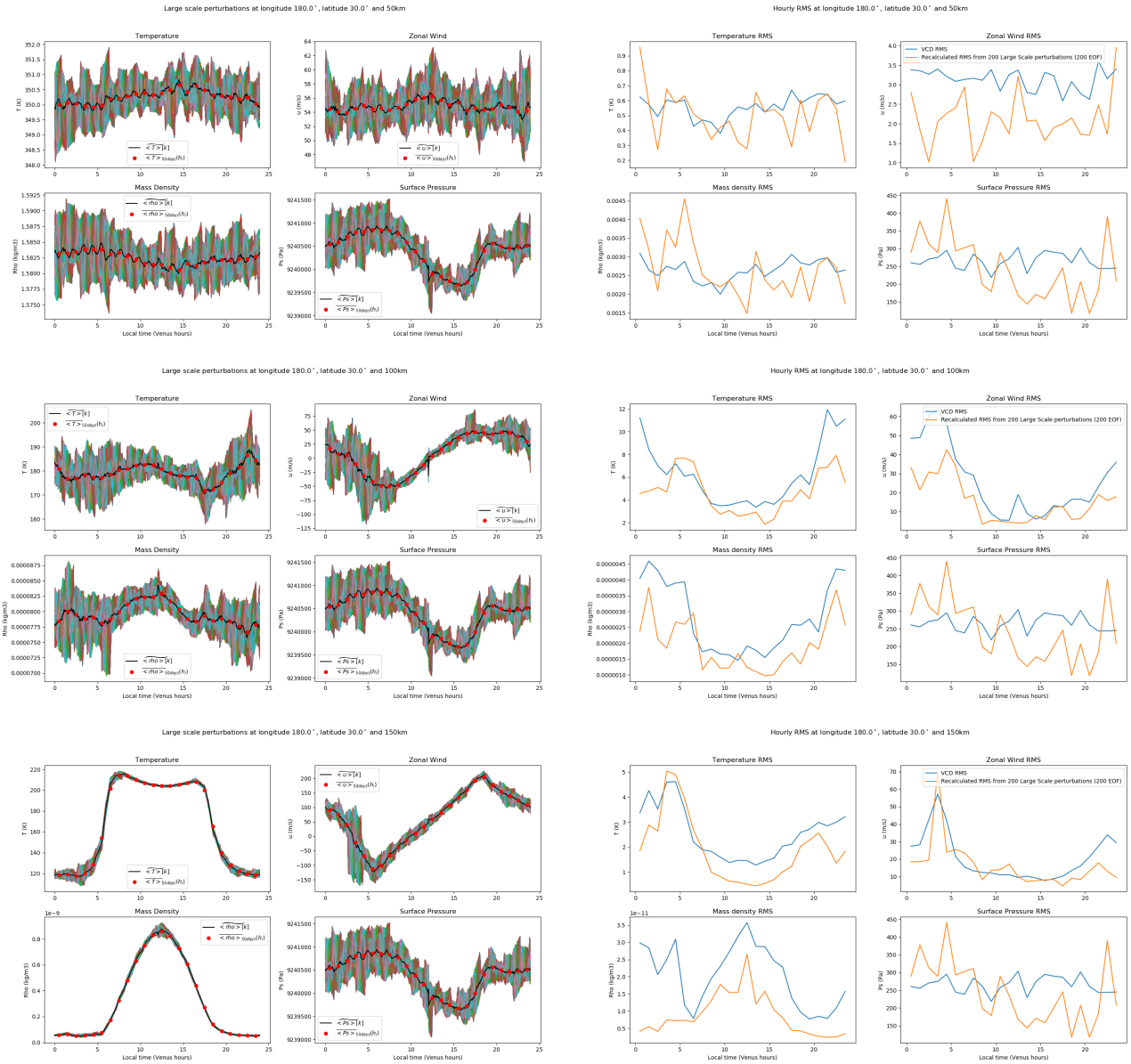

Figure 5: 50 simulated days with VCD using large scale perturbation mode (left) at longitude 180°, latitude 30° and altitude 50km (top), 100km (middle), 150km (bottom) for temperature, horizontal wind, density (recomputed) and surface pressure. Recalculated V-hourly RMS from these simulated days compared with V-hourly RMS stored in the VCD at the same point (right).

1.3 Illustration of gravity waves

The VCD includes also the possibility to add small scale perturbations, as gravity waves of which the user can choose the vertical wavelength (the horizontal wavelength being automatically computed as 100 times the vertical one). The parameterization of this gravity wave model is based on the one of the Mars Climate Database. These are non-orographic gravity waves emitted upward from the top of the cloud convective layer. The parameters were adjusted such that the amplitude of the wave in the VCD reproduces as best as possible the density wave amplitude observed with the Torque experiment during the VEXADE campaign. The comparison between these observations and the VCD using the same trajectory as Torque experiment with two different vertical wavelength (3 km and 5 km) is shown on Fig. 6. The scenario 7 was used with a E10.7 index of 102 s.f.u., which roughly corresponds to the UV solar flux recorded at the time of VEX-Torque measurements.

The over-estimation of the density at high latitudes is a bias of the VCD v2.0 that will be discussed in Section 2.2.3.

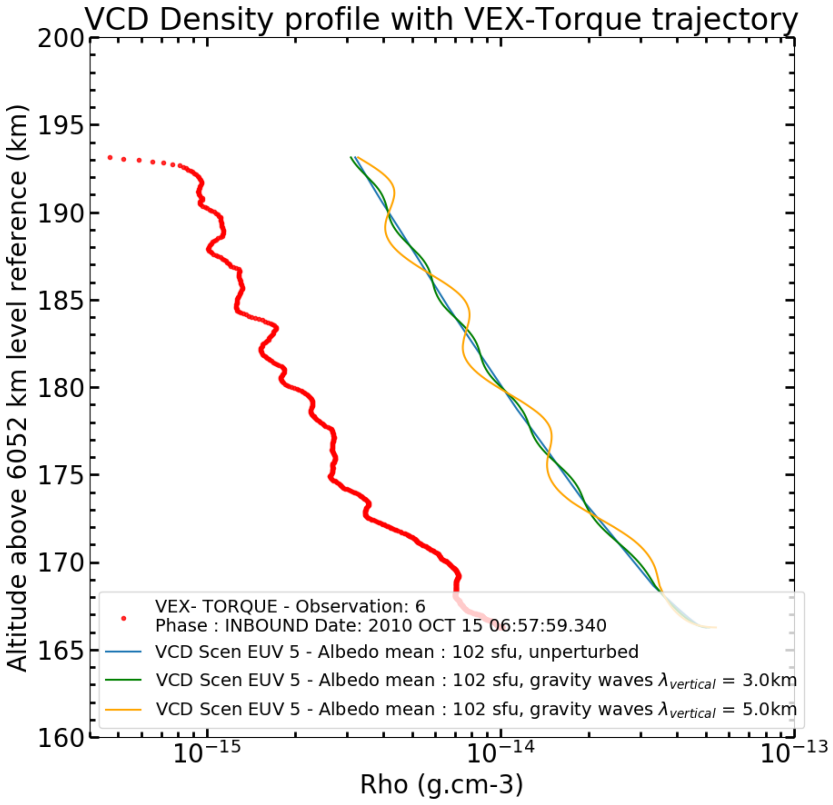

Figure 6: Density profiles from the VCD along VEX-Torque trajectory using small scale perturbations with a vertical wavelength of 3 km and 5 km and scenario 5 with E10.7 index of 102 s.f.u., compared with the corresponding density measurement during the VEXADE-Torque campaign.

2 Validation against observational datasets

The different variable profiles are extracted from the VCD for conditions corresponding to each of the observational datasets. The VenusGRAM profiles are also plotted for the same conditions, as extracted from the VenusGRAM (2005) software provided by NASA Justh et al. (2006).

2.1 Temperature

2.1.1 Deep atmosphere

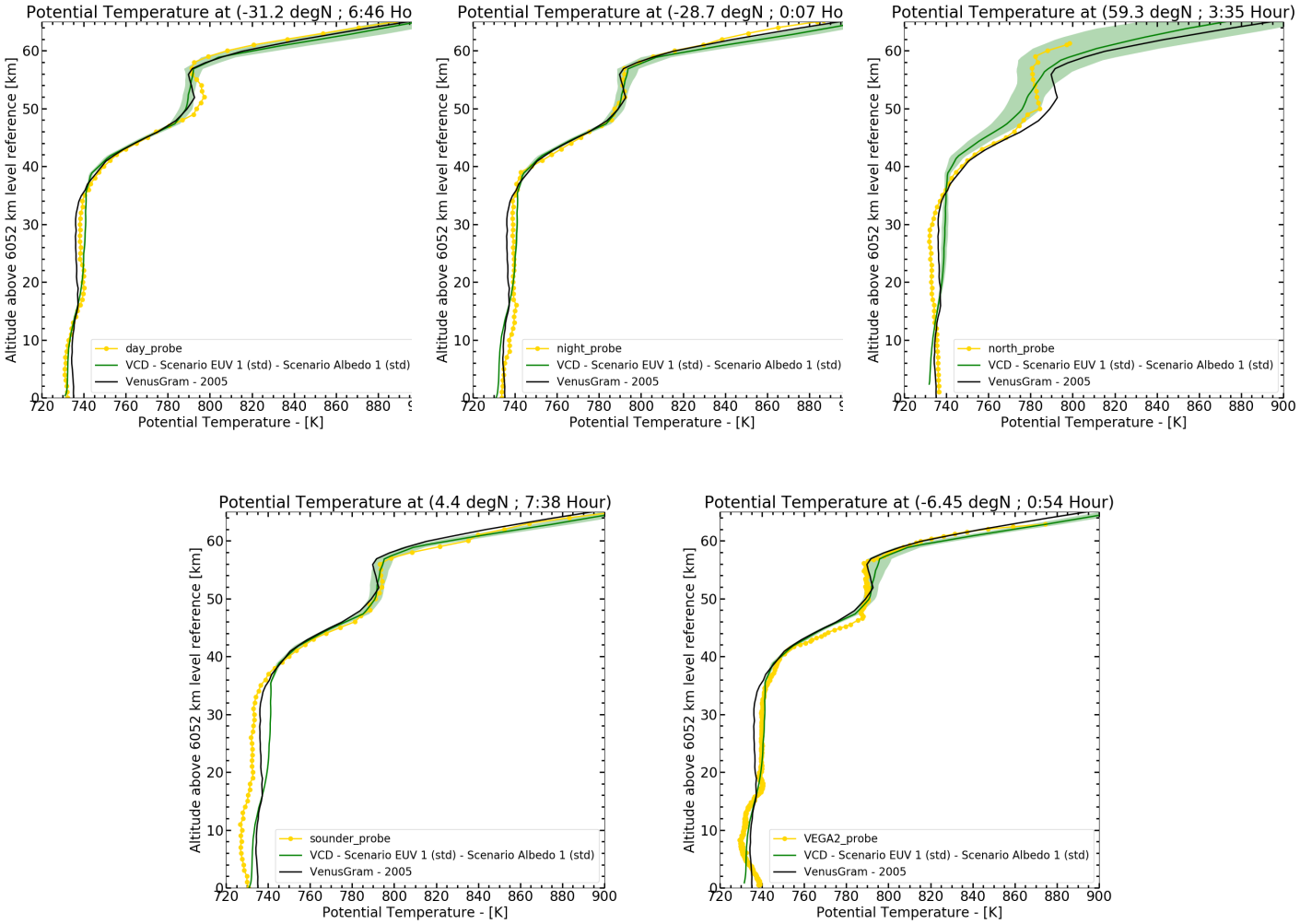

Figure 7: Potential temperature vertical profiles compared to Pioneer Venus and VeGa-2 probes.

In Fig. 7, the temperature profile is presented in the form of potential temperature for a better view of the vertical structure. Potential temperature is computed as detailed in Lebonnois et al. (2010). Profiles obtained by Pioneer-Venus probes are limited to above 12 km, but were extrapolated to the surface when published. In the VCD, there are only very small latitudinal variations in the temperature profiles. The significant differences among the probe profiles (mostly PV Sounder and PV North below 35 km) are therefore difficult to interpret. The variability present in the VCD in the cloud region for the PV North profile (59.3°N) is due to baroclinic wave activity that is strong at high latitudes. The VeGa-2 profile shows a peculiar instable region below 7 km, discussed in Lebonnois and Schubert (2017). This is not present in the VCD, as the possible origin of this peculiarity is still an open question.

2.1.2 Cold-collar region

The cold collar and its local time variations are well represented at 7×10^3 Pa (except that it reaches the pole at deeper pressures), as shown in Figs. 8 and 9. Above the cold collar, the VCD presents a secondary temperature minimum that is not present in the observations. It may be related to the description of the haze above the clouds in the solar and/or infrared spectra. Solving this will need a more detailed study.

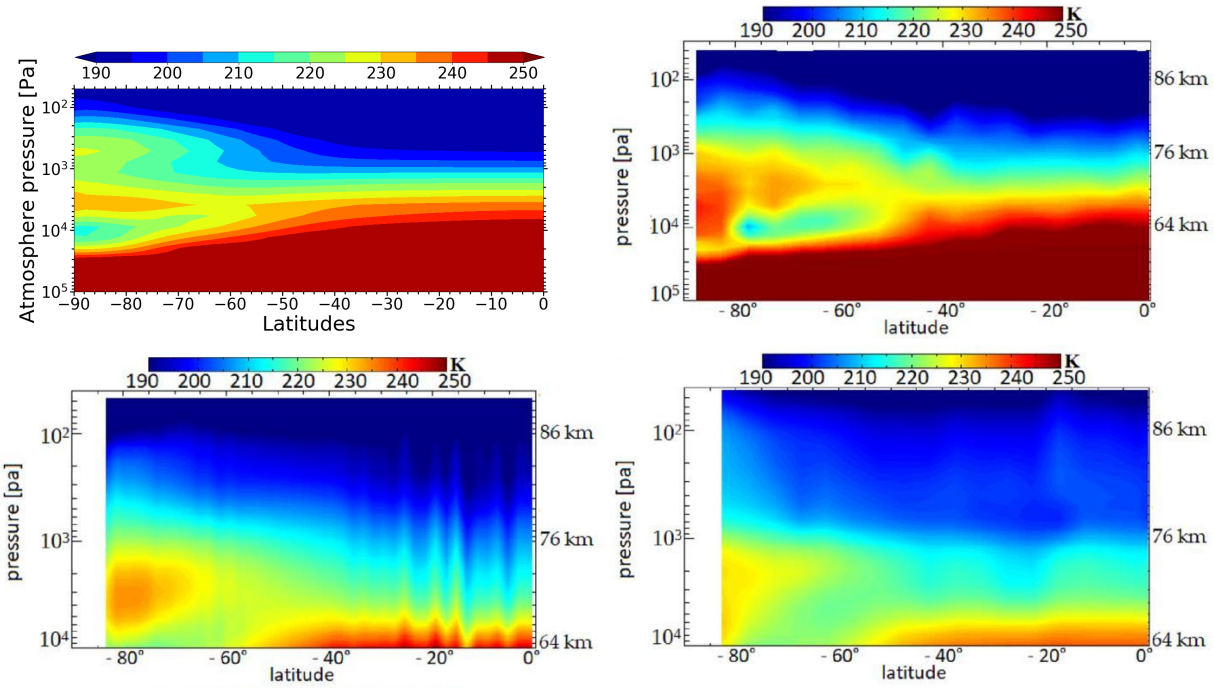

Figure 8: VCD cold-collar region temperature map compared to VIRTIS/Venus Express observations (VeRa, upper right; VIRTIS-M, lower left and VIRTIS-H, lower right). Average is done over all longitudes and over the night local times. From Scarica et al. (2019).

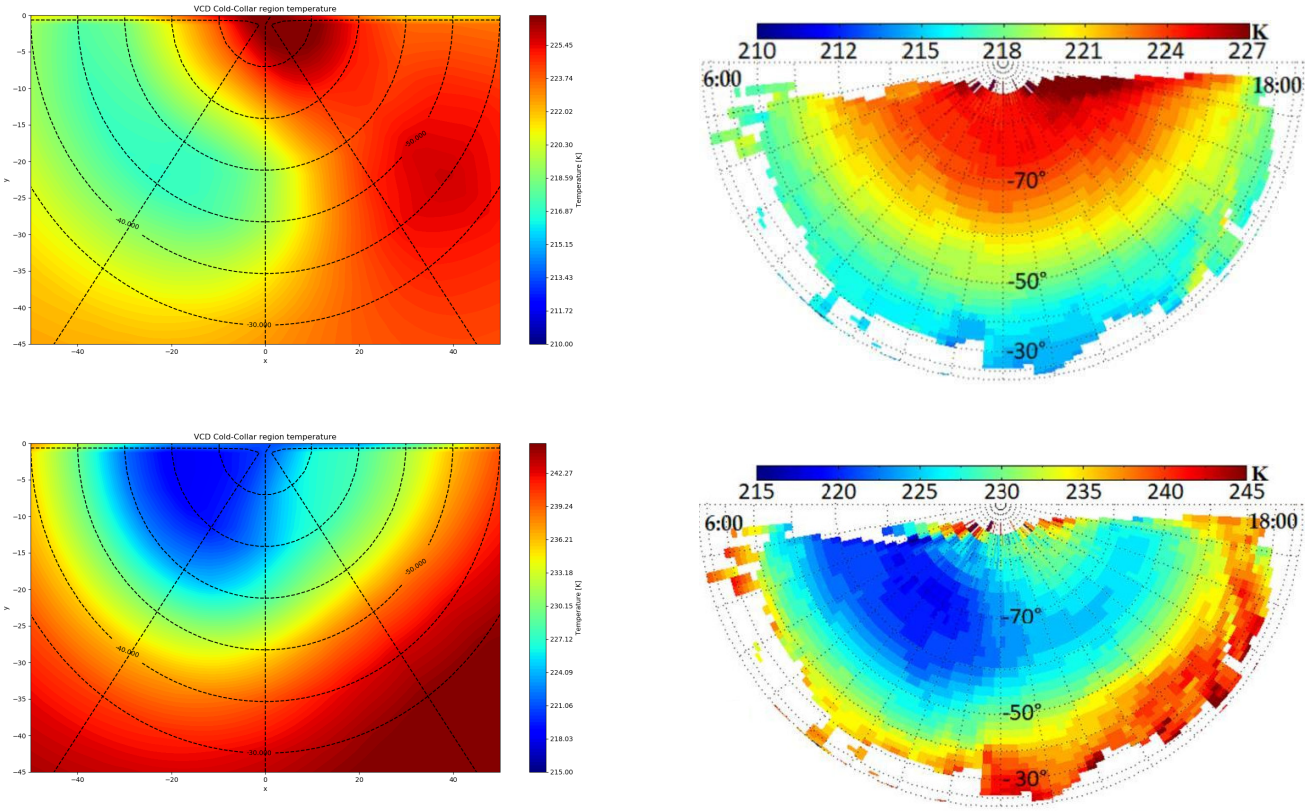

Figure 9: Night time polar temperature field at 2×10^3 (upper line) and 7×10^3 Pa (lower line) for the VCD (left row), compared to VIRTIS-M dataset (right tow). From Scarica et al. (2019).

2.1.3 Upper troposphere and mesosphere

The fit to the PV-OIR and PV-ORO datasets is good (Fig. 10), albeit the shape for the cold collar, as seen previously: the cold collar tends to reach the pole, and a secondary minimum is present between 75 and 80 km in the polar area.

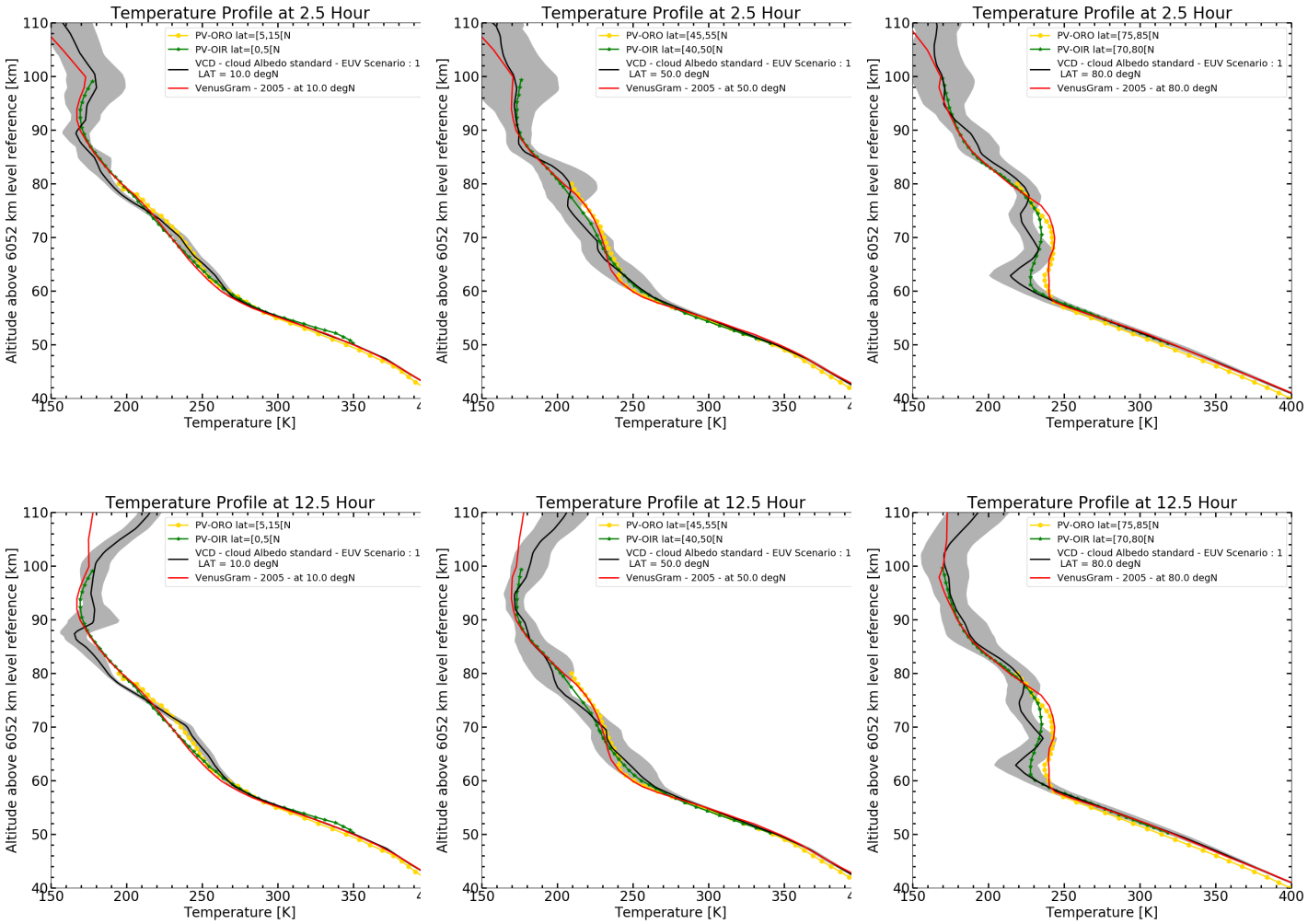

Figure 10: Comparison between the VCD temperature profiles, VenusGRAM and the PV-OIR and PV-ORO datasets at several latitudes (10, 50, 80°N), for LT=2.5 and 12.5.

2.1.4 Upper mesosphere - lower thermosphere

Despite the tuning that was done, some biases remain, as seen in Fig. 11:

- a cold bias is present on night time for high latitudes, between 0.1 and 0.01 mbar (10 to 1 Pa)
- for terminators, no local maximum is obtained near 10-2 mbar (1 Pa)
- on the dayside (and including terminators), a cold bias is present in upper thermosphere, above 130 km altitude. This is not seen in exospheric temperatures (see Fig. 12), therefore it may be possible that this is related to the vertical penetration of EUV solar flux in the GCM.

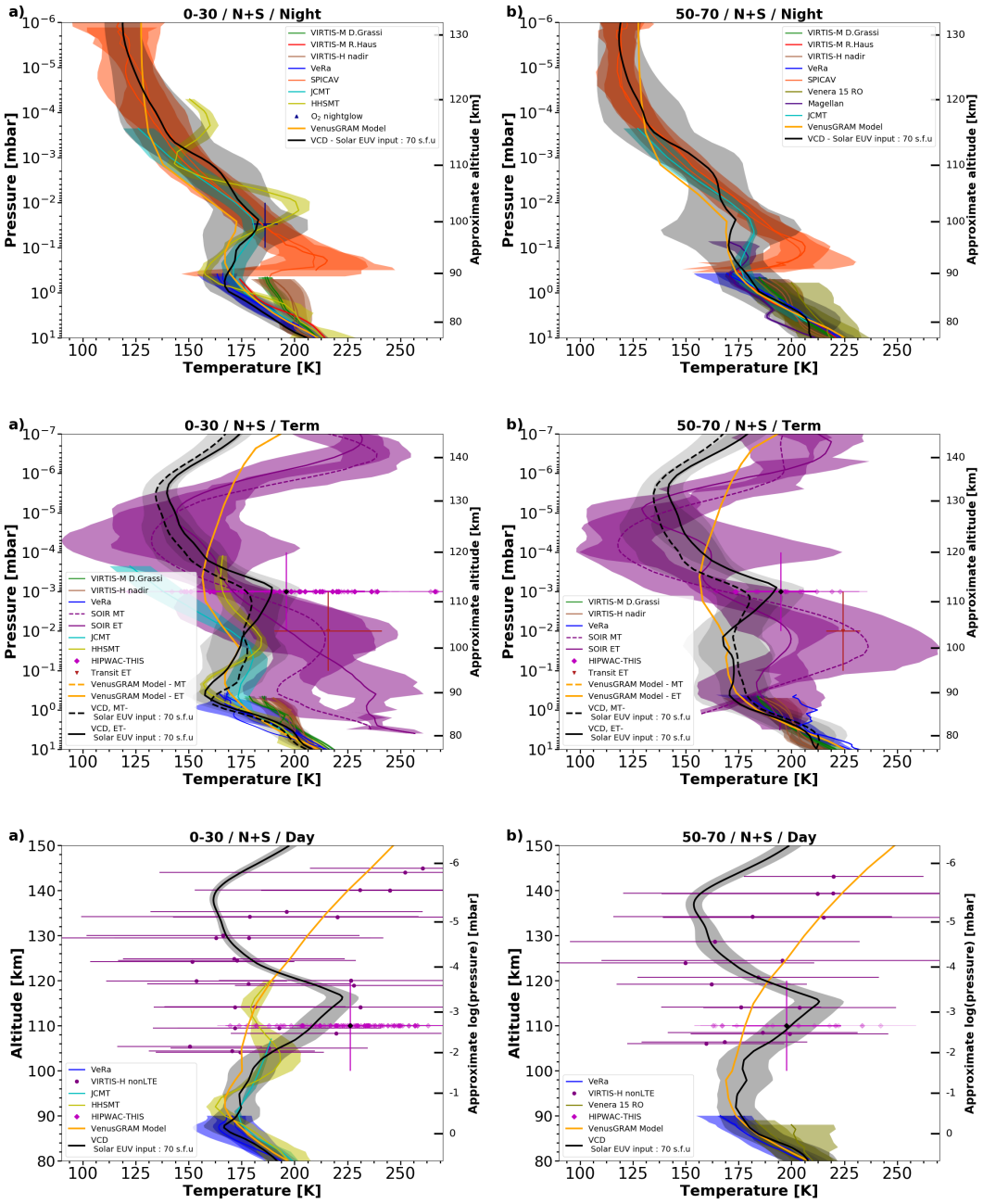

Figure 11: VCD temperature and VenusGRAM profiles compared to averaged temperature profiles observed by Venus Express and ground-based instruments for different local times (night/terminator/day) and latitude ranges (after Limaye et al. (2017)).

2.1.5 Upper thermosphere - Exosphere

The fit to exospheric temperatures is good on the dayside, as well as its dependency on E10.7 index (Fig. 12). However, the scattering of observed temperatures appear larger than the large-scale variability in the VCD. This may be related to small-scale perturbations, as seen in the Venus-Express VeXADE-Torque dataset (e.g. in Fig 6). On the nightside, the exospheric temperatures are well reproduced also, not depending on the E10.7 index, with the scattering of observed temperatures reproduced by large-scale variability, that is significantly larger on the nightside than on the dayside. However, as on dayside, small-scale gravity waves may also be active.

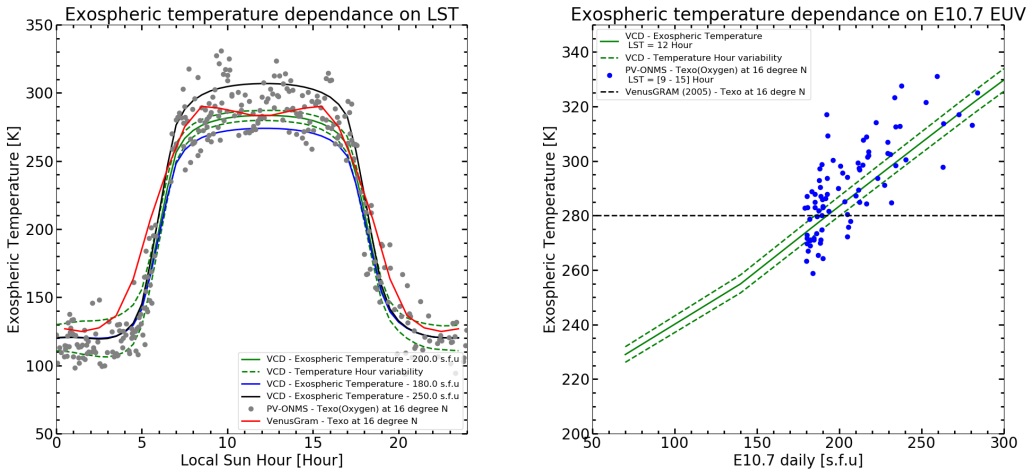

Figure 12: (left) Exospheric temperature as a function of local time, obtained from oxygen atom vertical scale height in the PV ONMS datasets, at E10.7 index ranging from 180 to 250, compared to the VCD profile for E10.7=215 (3-sigma hourly variability shown with dashed lines). Profiles at E10.7=180 and E10.7=250 are also included. (right) Exospheric temperature on the dayside as a function of the E10.7 index, obtained from oxygen atom vertical scale height in the PV ONMS datasets, compared to the VCD values. (3-sigma hourly variability shown with dashed lines). VenusGRAM does not take this sensitivity into account.

2.2 Mass density

2.2.1 Upper thermosphere - Pioneer-Venus

Near midnight ($\pm$2h LT), the mass density is slightly overestimated, by a factor up to 3, or a vertical shift upward by a few kilometers, as shown on Fig. 13. Variability, much larger in night time, seems to be well represented by the VCD.

2.2.2 Upper thermosphere - Magellan

Variability in the Precise Orbit Determination (POD) dataset is much larger than for the PV-OAD dataset, in particular on dayside, as we can see on Fig. 14. At these altitudes, densities are overestimated on the dayside only by a factor 2 to 3.

For the aerobraking dataset, in the comparison of Fig. 15, E10.7 index is taken according to the Earth date. In the 135-150 km range, the VCD overestimates the densities by 50 to 75% (slightly more between 14h and 16h), which corresponds to a vertical shift of roughly 1.8 km.

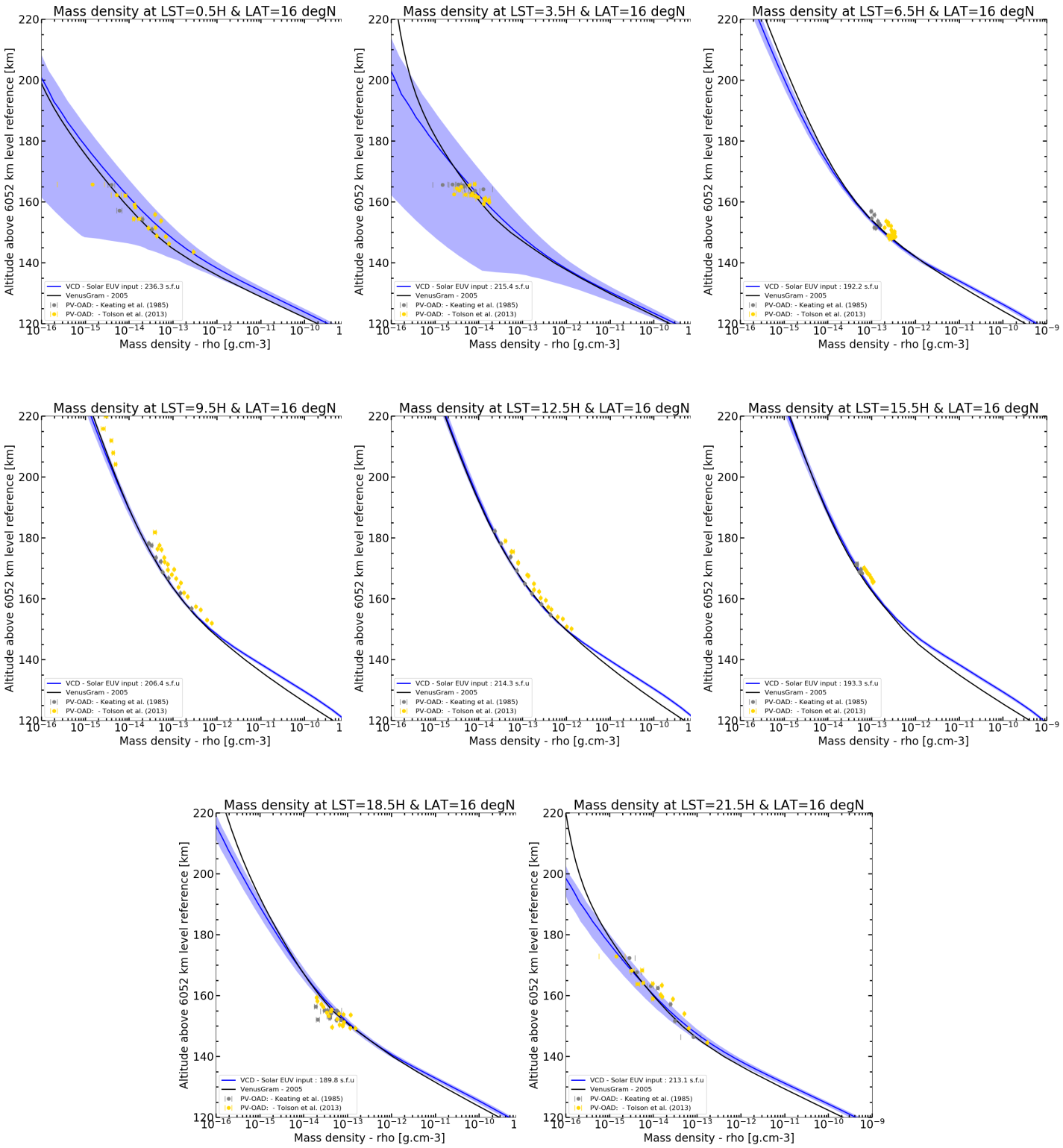

Figure 13: Comparison between the VCD profiles (including 3-sigma hourly rms in blue shade) for E10.7=236 s.f.u. (mean value corresponding to PV OAD observations) and densities retrieved by two different teams from PV OAD dataset (Latitude=16°). VenusGRAM is also shown in black. Local time goes from midnight (upper left) to 21h (lower right) by step of 3h.

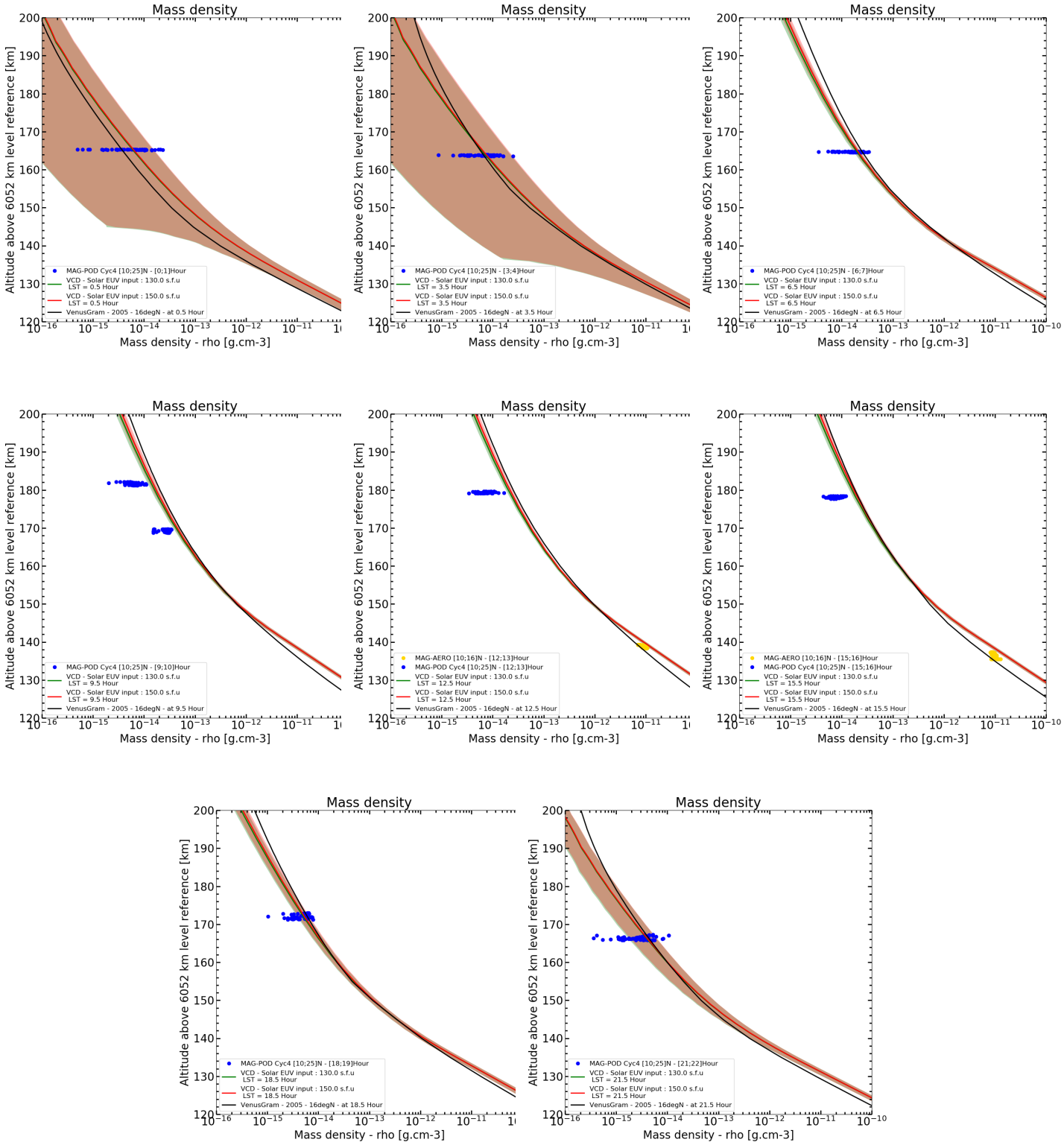

Figure 14: Comparison between the VCD profiles (including 3-sigma hourly rms in shades) for E10.7=130 s.f.u. (corresponding to Magellan aerobraking observations) and E10.7=150 s.f.u. (corresponding to Magellan POD observations), and densities retrieved by two different Magellan datasets, aerobraking (yellow, LT 10-18, latitudes 10-16°N) and POD (blue, latitudes 10-25°N). VenusGRAM is also shown in black. Local time goes from midnight (upper left) to 21h (lower right) by step of 3h.

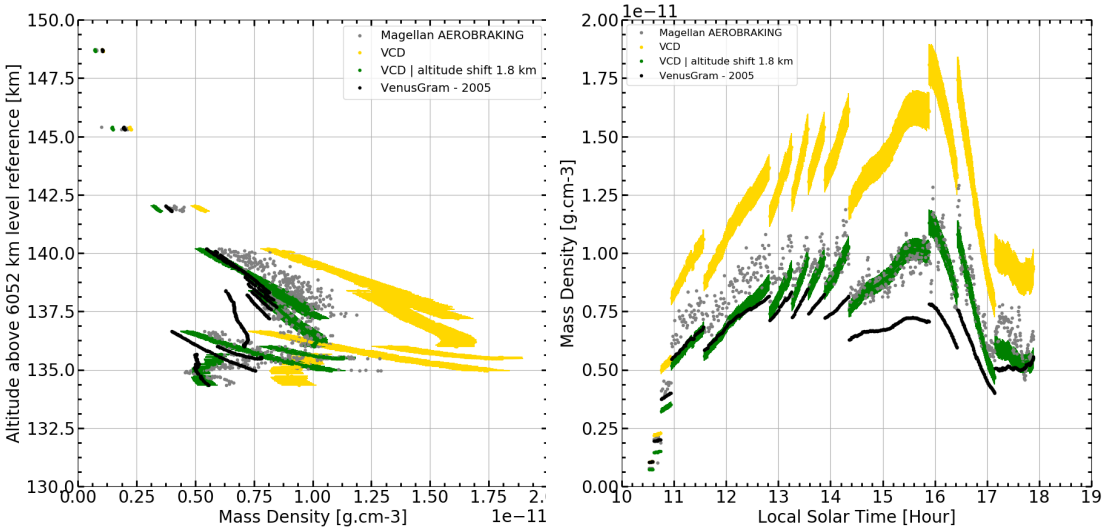

Figure 15: Comparison between Magellan aerobraking data (grey dots), the VCD (yellow, including the 1-sigma hourly + day-to-day rms) and VenusGRAM (black), density as a function of altitude (left) and local time (right). In green, the VCD values are taken 1.8 km higher than the corresponding observations.

2.2.3 Upper thermosphere - Venus-Express

During the VEXADE campaign, three types of experiments were performed: Torque, POD and Aerobraking, probing different altitude regions. Due to Venus-Express orbit, latitudes probed are close to the northern pole, and with local times close to terminator.

The variability observed in the VEXADE datasets may be mostly related to gravity wave activity. An example of using the VCD perturbation features to mimic this activity is shown on Fig. 16 (right panel). It may also be due to the E10.7 dispersion during measurements (with values up to 155 s.f.u. during the observation campaign).

An overestimation bias is seen in the VCD values for the polar regions, that might be related to a warm bias in the polar thermospheric temperatures.

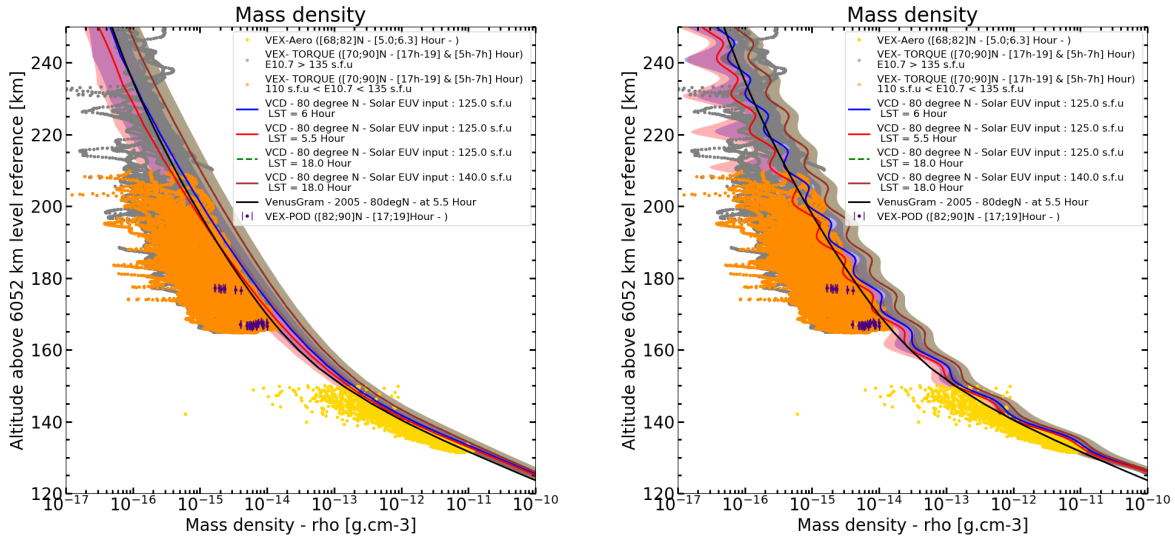

Figure 16: (left) Comparison between the VCD profiles at terminators (including 3-sigma hourly rms in shades) for E10.7=125 s.f.u. (mean value corresponding to VEXADE observations) and E10.7=140 s.f.u. (at evening terminator), and densities retrieved by the three experiments performed during the VEXADE campaign (Latitudes ranging from 68 to 90°N). VenusGRAM is also shown in black. Local time of observations is mostly between 5h and 7h (morning terminator), with some evening terminator data for the POD experiment. Several local times are plotted for the VCD, illustrating the variations during dawn. (right) Small-scale gravity wave perturbations are added on the VCD profiles.

2.2.4 Upper mesosphere, lower thermosphere

Comparison to Venus-Express datasets for mass densities in the 90-140 km region, nightside and terminators, is shown in Fig. 17. Consistency with observations is similar to VenusGRAM. At terminator and North polar latitudes, two individual examples of comparison between VEXADE-Aerobraking profiles and corresponding VCD profiles are shown in Fig. 18. Small-scale gravity waves (with vertical wavelength of 2 km) are included.

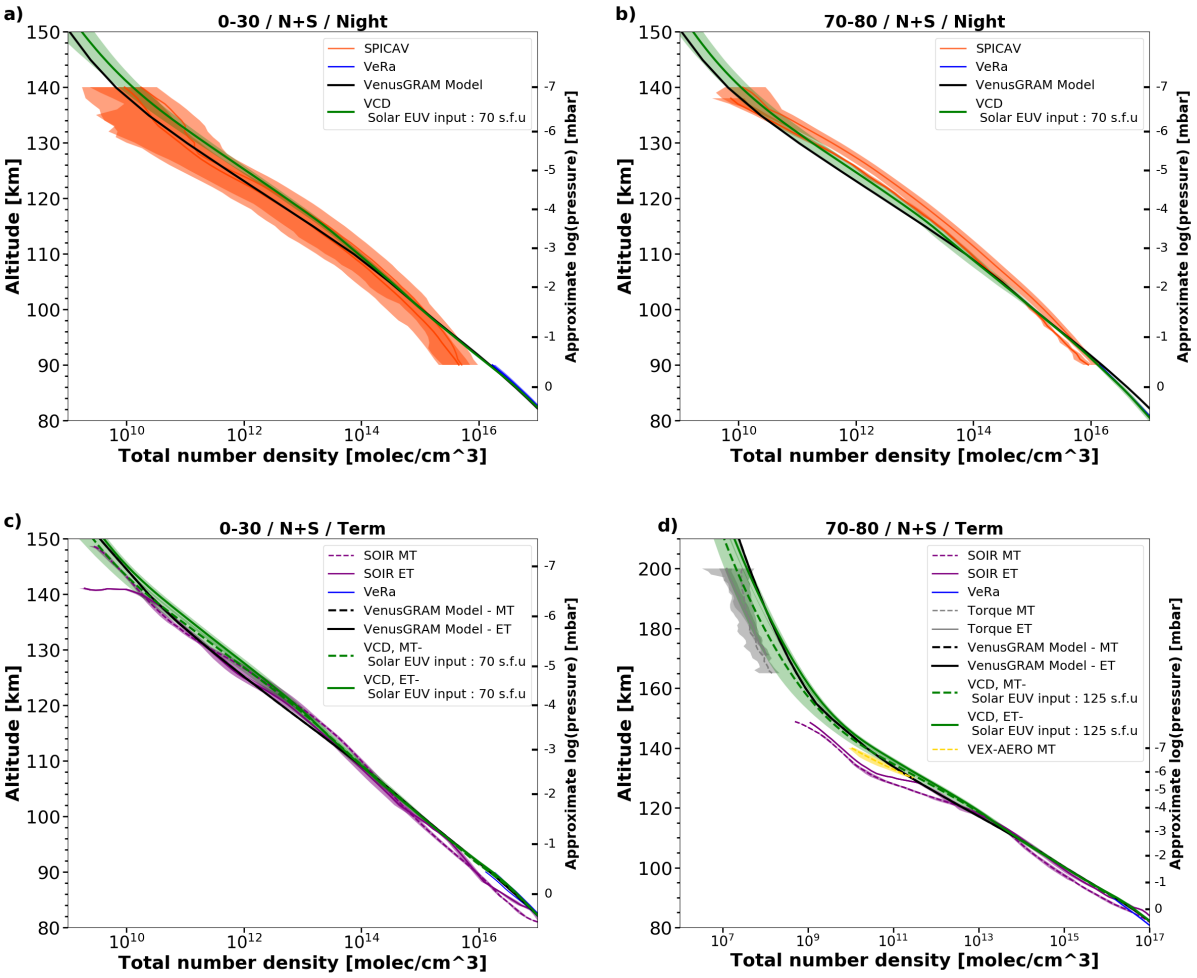

Figure 17: VCD and VenusGRAM number density profiles compared to averaged number density profiles observed by Venus Express for different local times (night and terminator) and latitude ranges (after Limaye et al. (2017)).

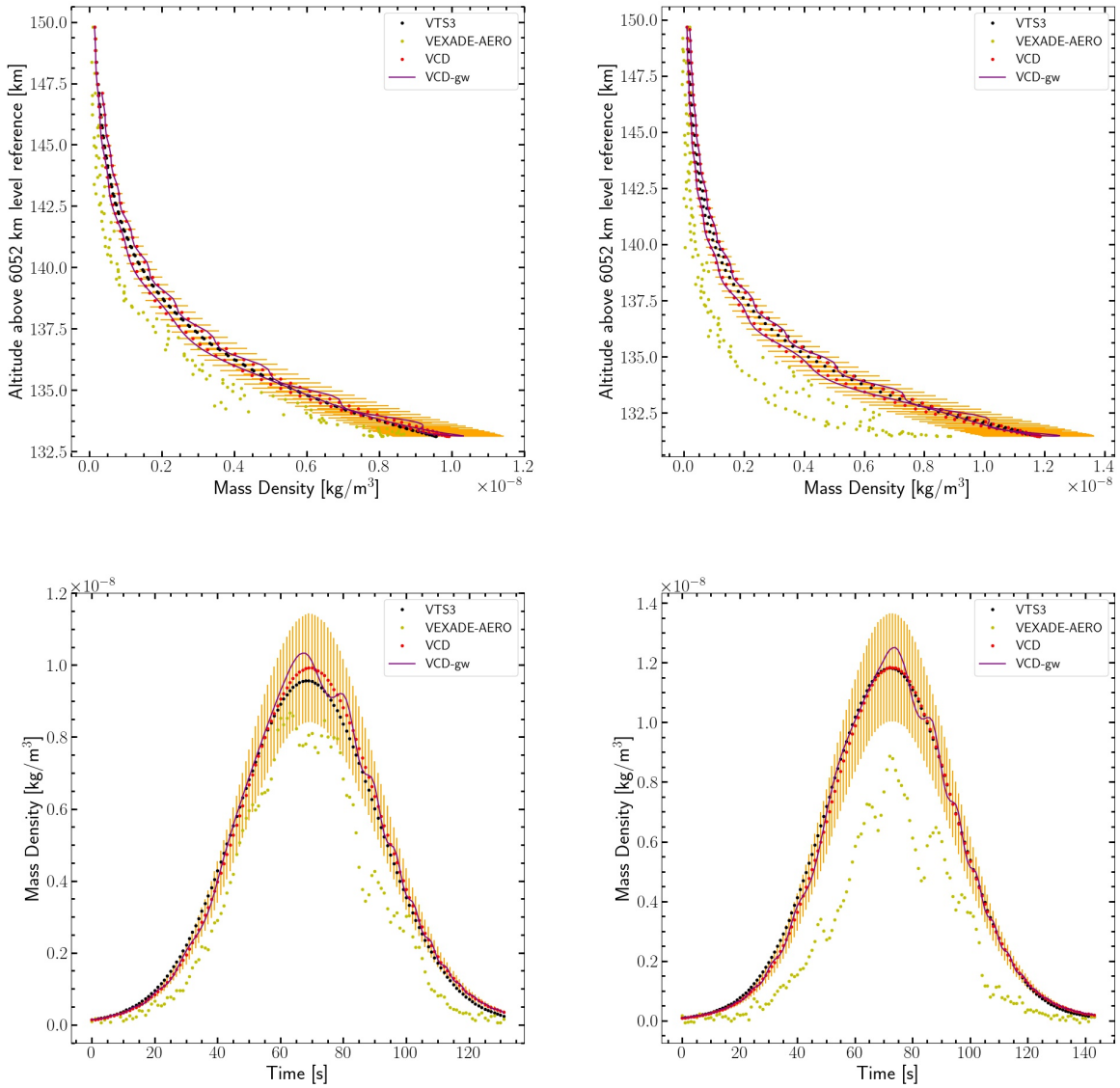

Figure 18: Density profiles from the VCD along VEXADE-Aerobraking trajectories (n° 624 on left and 705 on right) using small scale perturbations with a vertical wavelength of 2 km, EUV scenario 5 with E10.7 index corresponding to observations and standard albedo scenario, compared with the corresponding density measurement during the VEXADE-Aerobraking campaign and VTS3 model values.

2.3 Composition

2.3.1 Upper thermosphere

Number density profiles for the different constituents shows a large variability on the nightside, consistent with the variability observed in the total mass density (see Fig. 13). As shown on Fig. 19, there appears to be a bulge of Helium increasing from 1h to 4h (nighttime), retreating with a large spread around 5h (morning terminator). This is not represented in the VCD. The agreement is satisfying, though a slight underestimation of O atoms is visible on dayside.

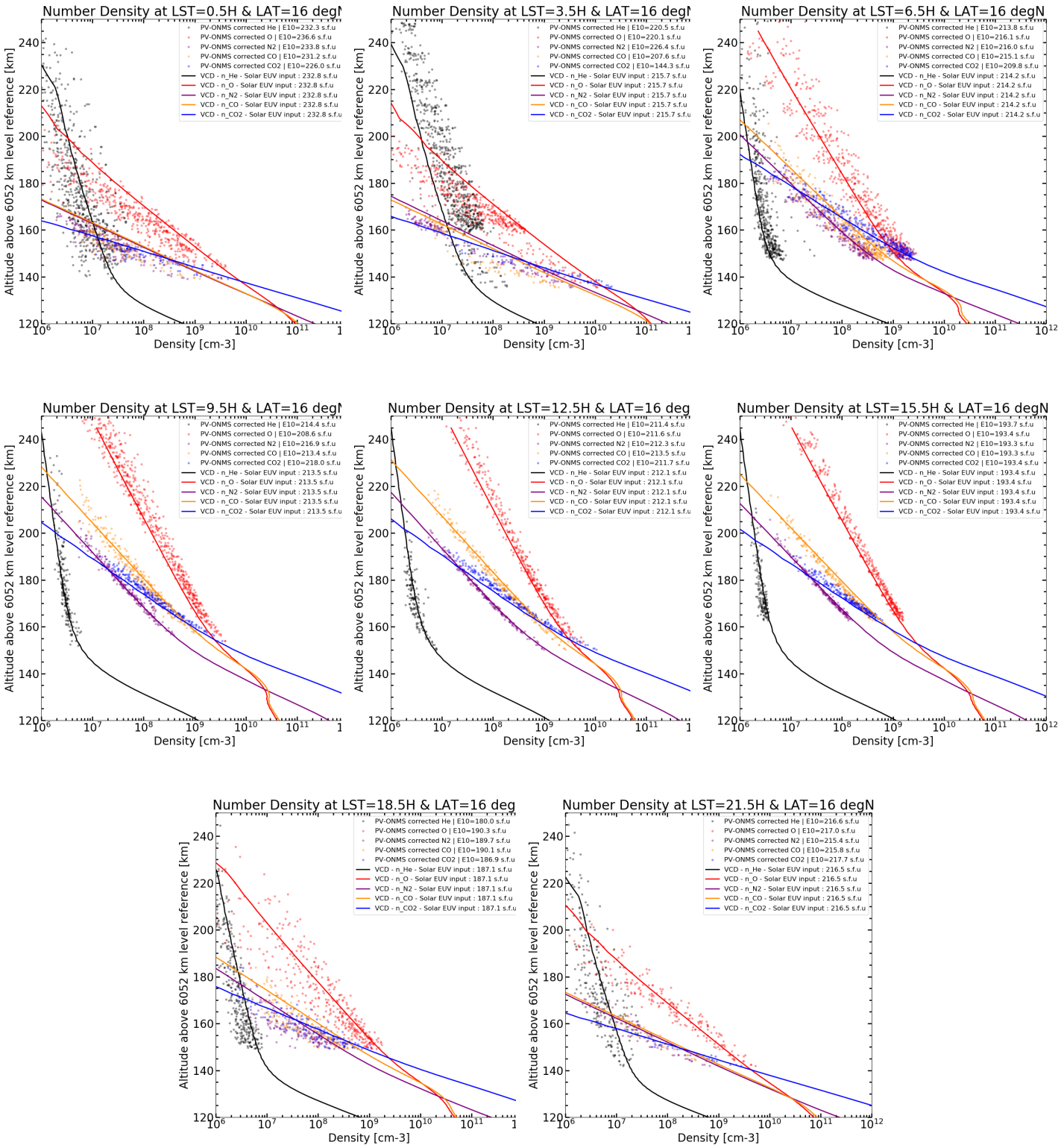

Figure 19: Vertical profiles of the number densities of He (black), N2 (purple), CO2 (blue), CO (yellow) and O (red) observed by PV-ONMS (including a correcting factor as recommended by Keating et al. (1985) for the VIRA model), compared to VCD profiles, for low latitudes (0-30°) and local times from midnight to 21h, every 3h. The "PVO-V-ONMS-4-NEUTRALDENSITY-12SEC-V1.0" and "PVO-V-POS-5–VSOCOORDS-12SEC-V1.0" are obtained from the Planetary Data System (PDS) (https://pds.nasa.gov/).

2.3.2 Thermospheric CO profiles

For CO density profiles, the difference due to the E10.7 index (different between the two periods of observations) is visible only above roughly 160 km (see Fig. 20). Below 120 km, the CO density profile is much closer to the observations than the VenusGRAM profile.

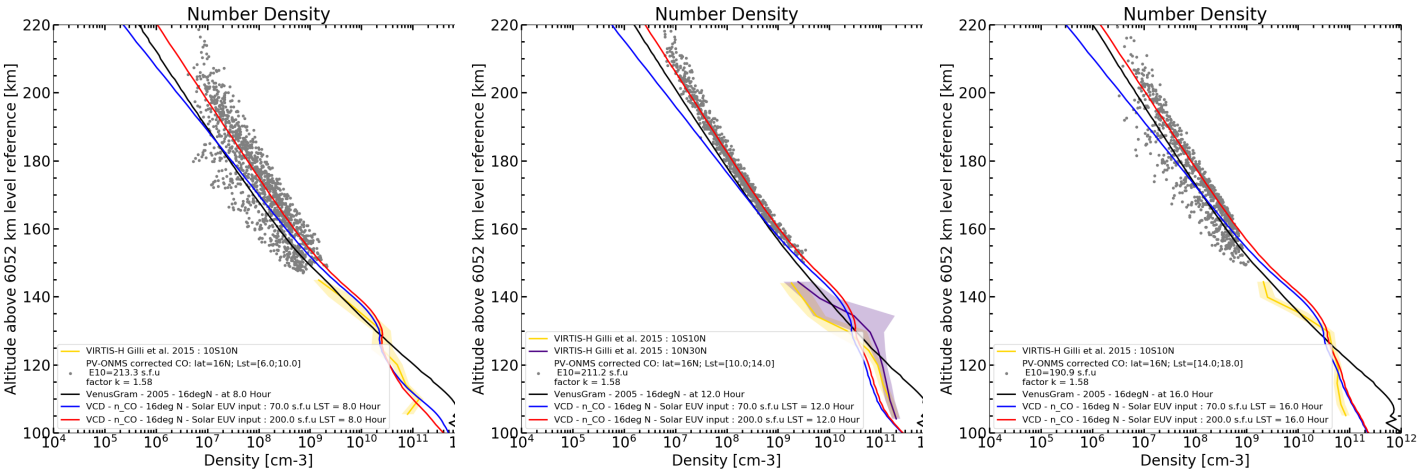

Figure 20: VCD profiles of CO number density at E10.7=200 s.f.u. (red) and 70 (blue) (variations above 160 km) for three local times (8h, 12h and 16h), compared to PV-ONMS data and retrievals from analysis of VIRTIS-H spectra, and VenusGRAM profiles (black).

2.3.3 Mesospheric O Profiles

In their analysis of the oxygen nightglow, Soret et al. (2012) retrieved O density profiles in the 85-110 km altitude range. In their Fig. 7, they show a particular profile obtained for conditions LT=00:44 and latitude=24°S. This profile is compared in Fig. 21 to the corresponding profile extracted from the VCD (averaged over longitudes). The VCD overestimates by a factor of roughly 2 the O density near the peak, though its altitude is a few km higher than observed.

2.3.4 H_2O and SO_2 Profiles

The tuning of SO_2 above and below the clouds is extremely sensitive. Deep atmosphere SO_2 vmr needs to be fixed an order of magnitude below observations, otherwise the abundance above the clouds are several order of magnitudes higher than observations... Therefore, sulfur compounds are not reliable in the VCD for the moment.

Profiles for H_2O and SO_2 are shown in Fig. 22. Water vaper vmr are approximately satisfying, though also dependent on SO_2 abundance above the clouds, which is too high in these figures by roughly an order of magnitude.

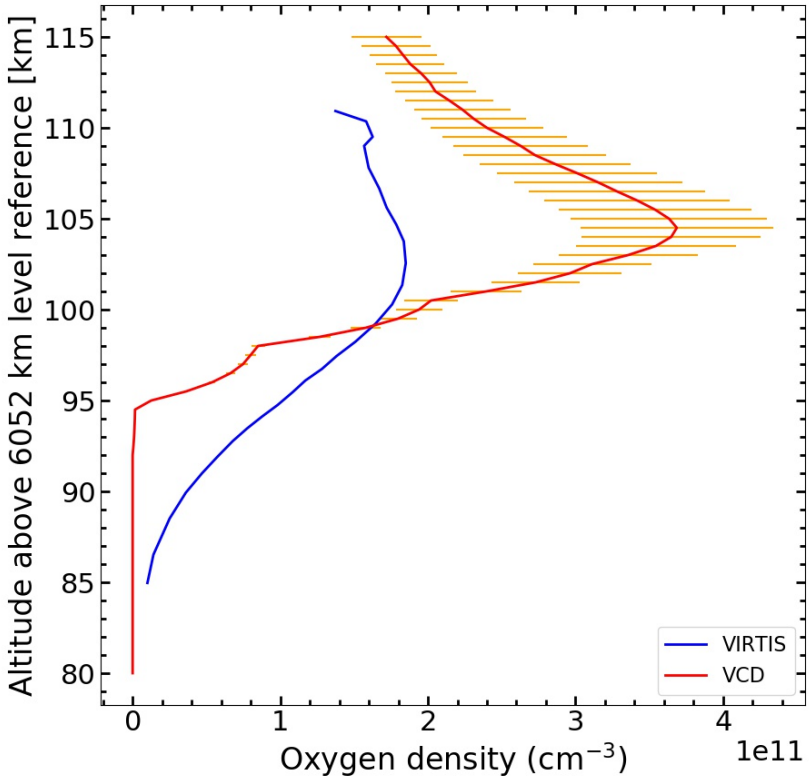

Figure 21: VCD vertical profile of O density at LT=00:44, latitude=24°S, compared to values retrieved from VIRTIS/VenusExpress (Soret et al., 2012).

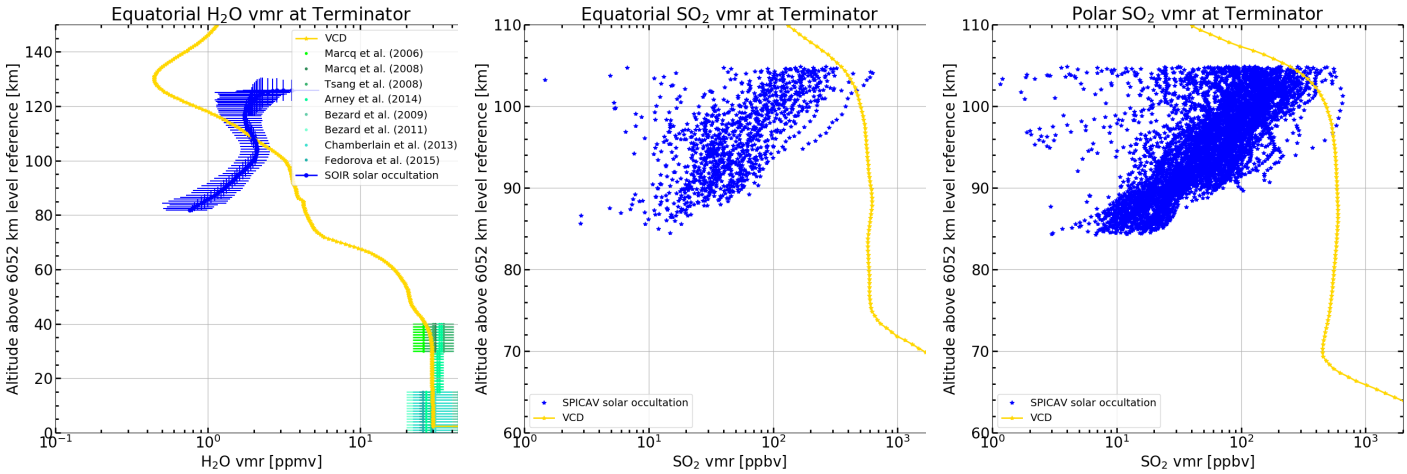

Figure 22: (left) Water vapor vmr profile compared to various observational datasets. (center) SO_2 vmr profile near equator at terminator compared to SPICAV/Venus EXpress dataset. (right) same for polar region.

2.3.5 Electron density

The electron density is an addition to the VCD version 2.2. As shown in Fig. 23, the evolution of the vertical electron profile is quite consistent with the PV-OETP observations between 150 and 190 km altitude although at the terminator we overestimate the electron density above 180 km.

Figure 24 dislays the peak electron density and the peak electron altitude as a function of the SZA for the main Chapman layer. The agreement is satisfactory with the observations of the Pioneer Venus mission (high solar activity around 200 s.f.u). Despite a slight overestimation of the peak density that is visible for the low solar activity at noon (5.7 vs. 5., Fig. 24), the electron density from the VCD is able to reproduce the zonal evolution on dayside.

The electron model present for VCD 2.2 is valid between 100 and 190 km on dayside. Above this altitude, electromagnetic processes such as ambipolar scattering (a process not included in the GCM) is no longer negligible compared to the dissociative recombination process, which causes electron accumulation that starts to be visible at the terminator at 190 km where the recombination process is weaker. Below 100 km, the model scatters the electrons as a species in the absence of electromagnetic destruction process, which will tend to overestimate the electron density. A similar effect is at work on the nightside.

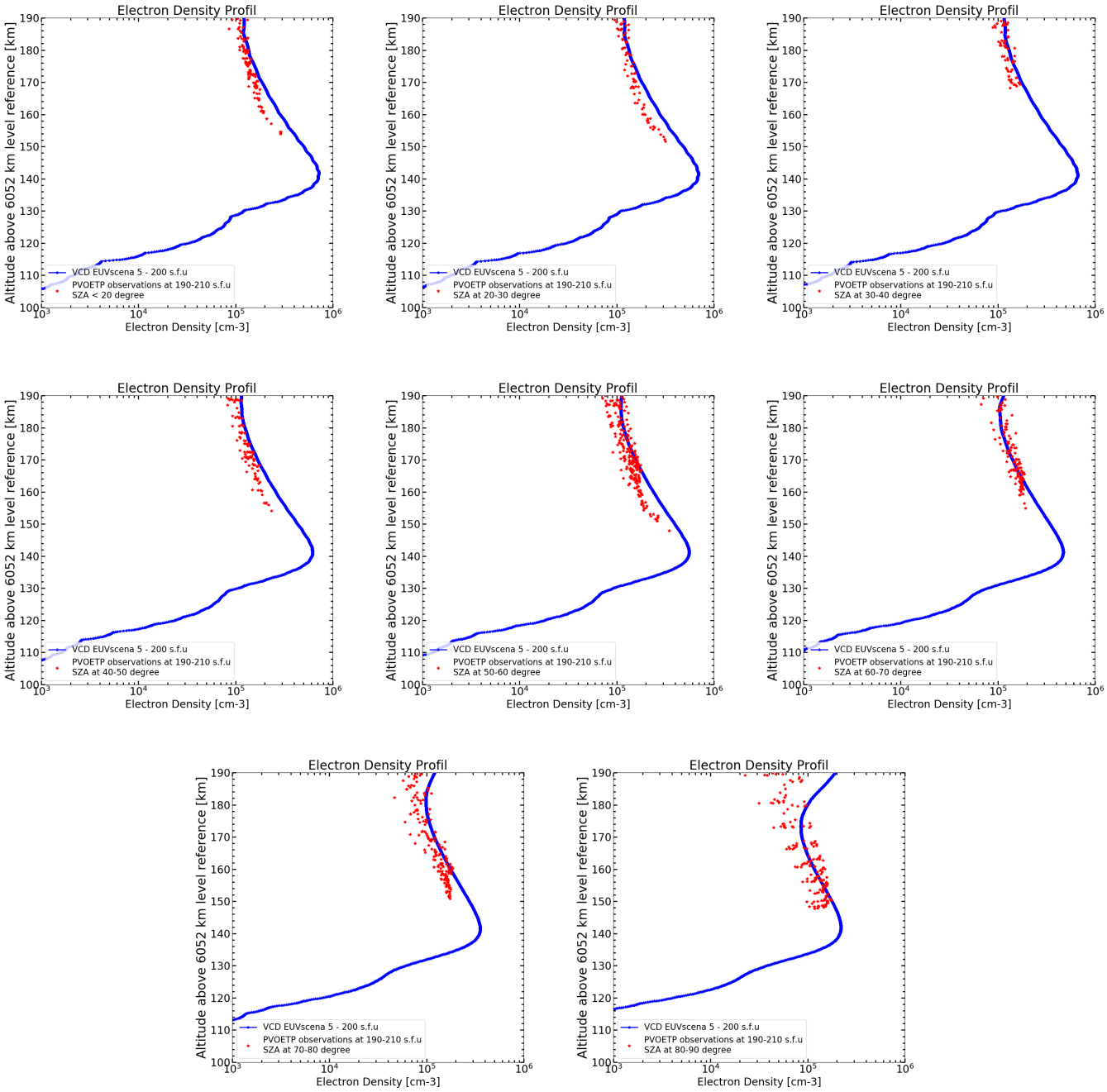

Figure 23: Vertical profiles of the electron number density (blue), using EUV scenario 5 with E10.7 index at 200 s.f.u corresponding to observations, compared to Pioneer-Venus Orbiter Electron Temperature Probe (PV-OETP) measurements for different latitude ranges. The ”PVO-V-OETP-5-LORESELECTRONS-V1.0” and ”PVO-V-POS-5–VSOCOORDS-12SEC-V1.0” are obtained from the Planetary Data System (PDS) (https://pds.nasa.gov/).

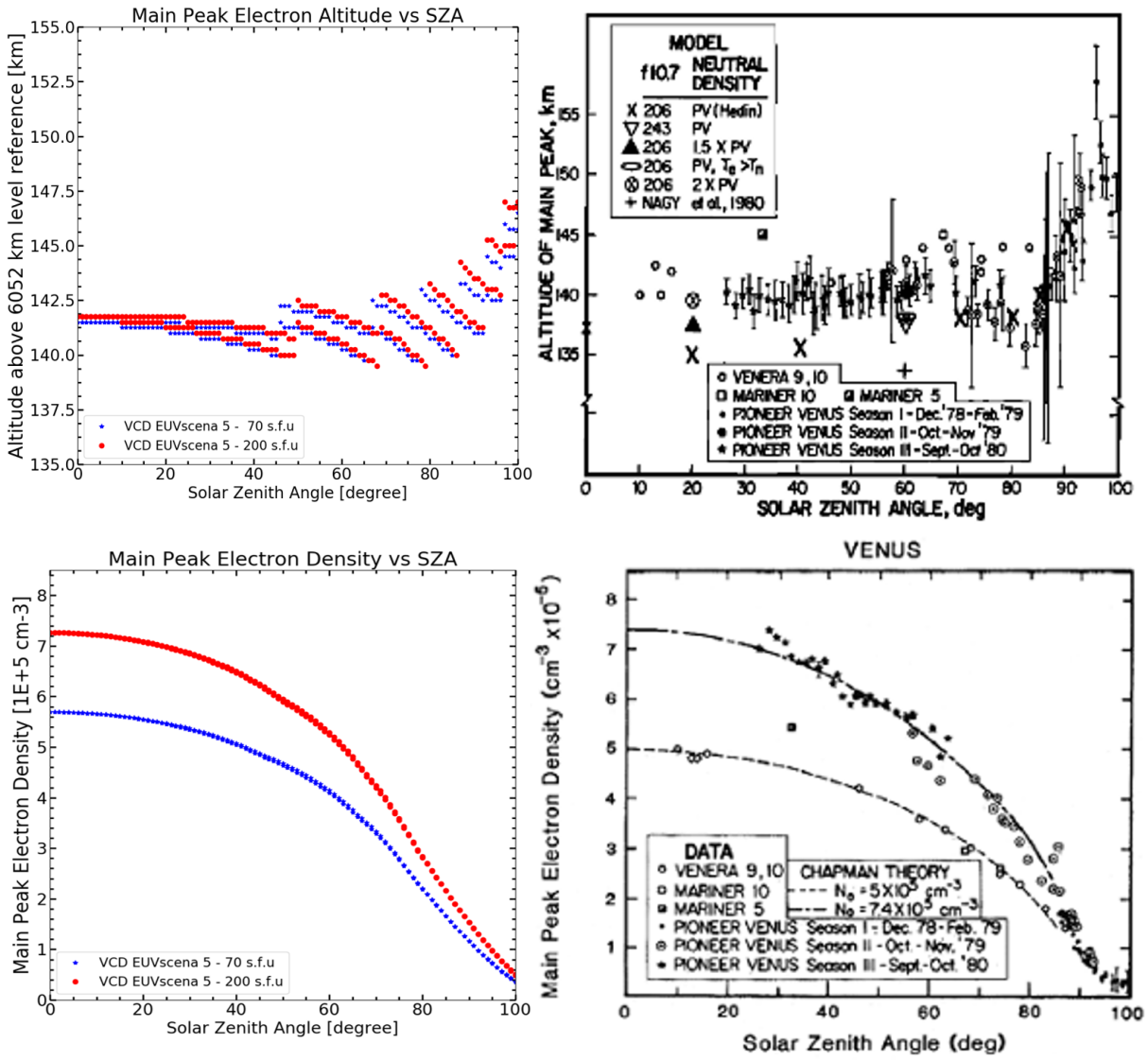

Figure 24: Altitude and electron density at peak as a function of solar zenith angle for high (E10.7=200 s.f.u., red) and low (E10.7=70 s.f.u., blue), compared to observations. Right panels are from Cravens et al. (1981), according to the observations of the Mariner, Pioneer Venus and Venera missions for high and low solar activity.

2.4 Exosphere

In addition to the bulge of He discussed in previous section, some analyses of Ly α observations give access to H densities in the exosphere. A bulge of H is seen in the observations near 4h in the late night (for altitudes around 250 km), and there seem to be an asymmetry between morning and evening terminators. Both characteristics are present in the VCD, as seen in Fig. 25, though with an order of magnitude less enhancement for the bulge. The H abundance in the exosphere is overestimated in the VCD by a factor roughly 2.

2.5 Zonal and meridional winds

2.5.1 Cloud region and below

At low latitudes (up to roughly 45°), the zonal wind does not vary much with latitude (see also Fig. 26), and its vertical variation seems to be consistent with cloud-tracking measurements (see also Fig. 27). For

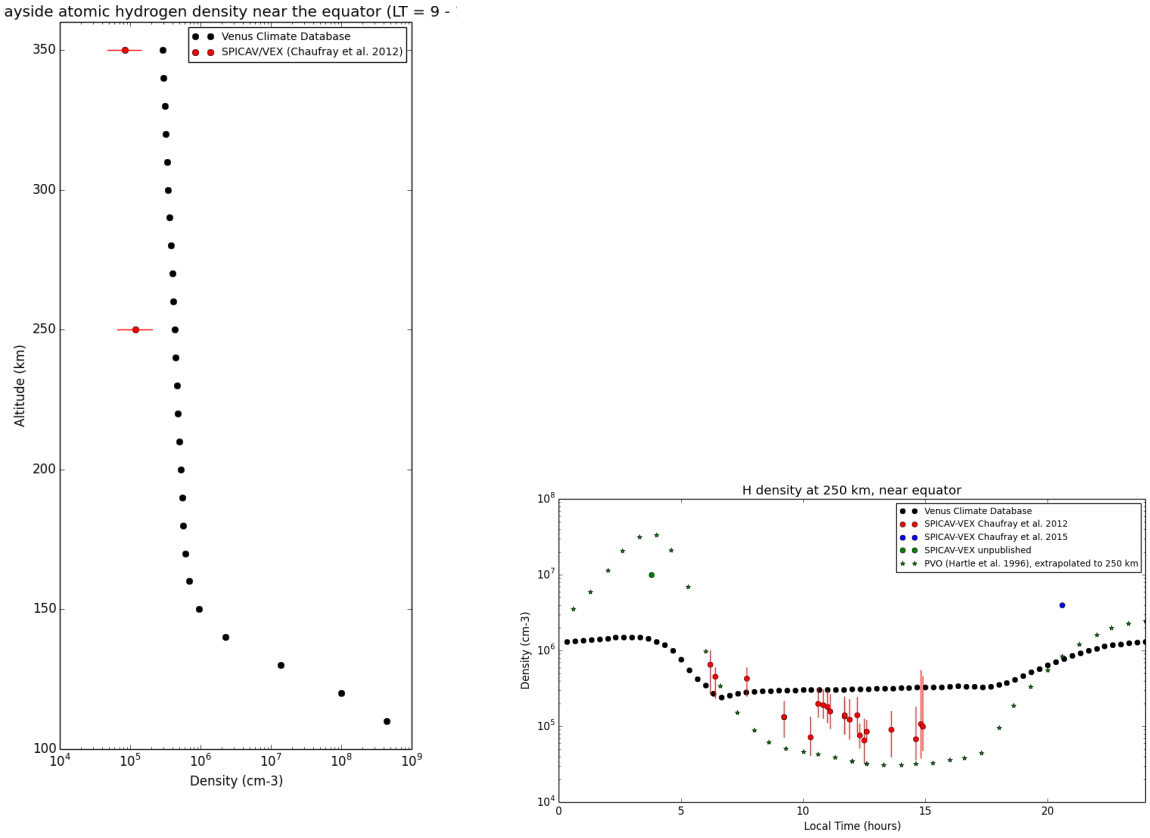

Figure 25: (a) VCD vertical profiles of H density on the dayside near the equator, compared to values retrieved from SPICAV/VenusExpress (Chaufray et al., 2012). (b) VCD local time variations of H density at 250 km altitude near the equator, compared to available observations.

higher latitudes, the jet seen in the VCD near 65° latitude is not present in the observations. It must be noted that the altitude of the cloud-tracking layers is going down slightly when going towards the poles, which may affect the comparison. The poleward shift of the modeled jets compared to observations is one of the VCD most significant bias.

The VCD zonal wind profile follows the observed trends for the deep atmosphere, though the amplitude is beyond observed values.

2.6 VeGa Balloons

The VeGa balloons observed variability in the vertical winds. However, it is not possible to directly compare to the VCD (even the rms values), since these observed variations are related to convective activity that is not explicitly represented in the GCM simulations. Only LES experiments can reproduce these observations, see Lefèvre et al. (2018).

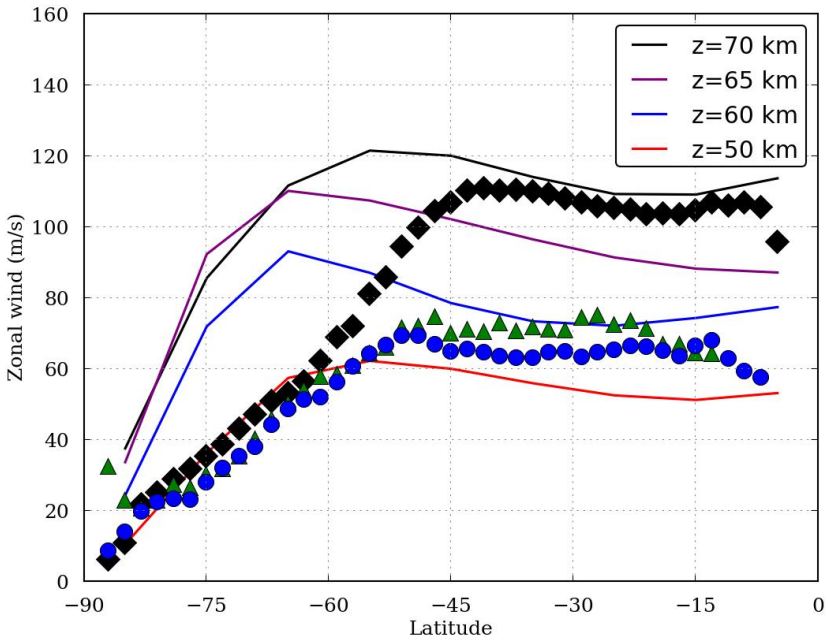

Figure 26: Latitudinal profiles of zonal wind at several levels in the clouds. Symbols correspond to VIRTIS/VenusExpress observations (Hueso et al. (2015)) : black diamonds for UV cloud-tracking features (66-72 km), green triangles for visible features, blue circles for Near-IR features (58-63 km).

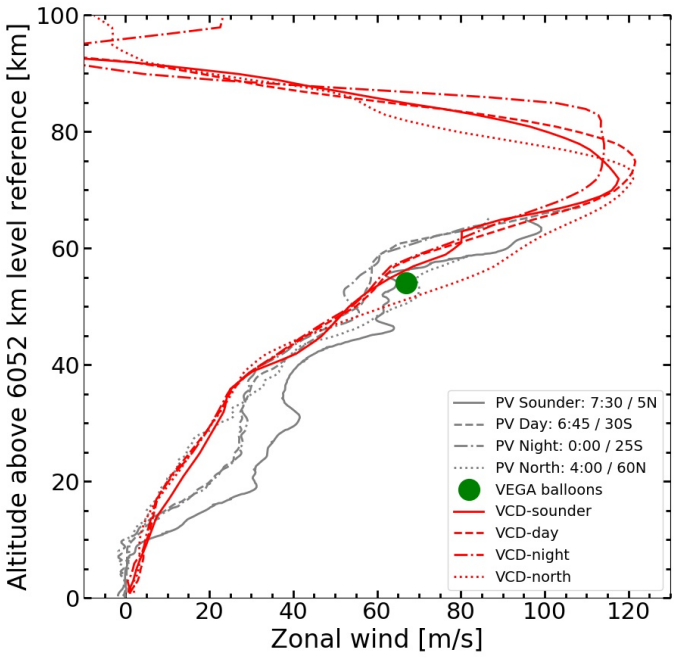

Figure 27: Vertical profiles of zonal wind compared to profiles observed by the Pioneer Venus entry probes. The average zonal wind speed measured by the two VeGa balloons is also indicated with the green disk. Local time and latitudes are indicated in the legend for each probe.

References

Chaufray, J.-Y., Bertaux, J.-L., and Leblanc, F. (2012). First observation of the Venus UV dayglow at limb from SPICAV/VEX. *Geophys. Res. Lett.*, 39.

Cravens, T. E., Kliore, A. J., Kozyra, J. U., and Nagy, A. F. (1981). The ionospheric peak on the Venus dayside. *J. Geophys. Res.*, 86(A13):11323–11329.

Hueso, R., Peralta, J., Garate-Lopez, I., Bandos, T. V., and Sánchez-Lavega, A. (2015). Six years of Venus winds at the upper cloud level from UV, visible and near infrared observations from VIRTIS on Venus Express. *Planet. & Space Sci.*, 113-114:78–99.

Justh, H. L., Justus, C. G., and Keller, V. (2006). Global Reference Atmospheric Models, Including Thermospheres, for Mars, Venus and Earth. In *AIAA/AAS Astrodynamics Specialist Conference and Exhibit*, page 6394.

Keating, G. M., Bertaux, J. L., Bougher, S. W., Dickinson, R. E., Cravens, T. E., Nagy, A. F., Hedin, A. E., Krasnopolsky, V. A., Nicholson, J. Y., Paxton, L. J., and von Zahn, U. (1985). Models of Venus neutral upper atmosphere: Structure and composition. *Adv. in Space Res.*, 5(11):117–171.

Lebonnois, S., Hourdin, F., Eymet, V., Crespin, A., Fournier, R., and Forget, F. (2010). Superrotation of Venus' atmosphere analysed with a full General Circulation Model. *J. Geophys. Res.*, 115:E06006.

Lebonnois, S. and Schubert, G. (2017). The deep atmosphere of Venus and the possible role of density-driven separation of CO_2 and N_2. *Nature Geosci.*, 10:473–477.

Lefèvre, M., Lebonnois, S., and Spiga, A. (2018). Three-Dimensional Turbulence-Resolving Modeling of the Venusian Cloud Layer and Induced Gravity Waves: Inclusion of Complete Radiative Transfer and Wind Shear. *J. Geophys. Res. Planets*, 123:2773–2789.

Limaye, S. S., Lebonnois, S., Mahieux, A., Pätzold, M., Bougher, S., Bruinsma, S., Chamberlain, S., Clancy, R. T., Gérard, J.-C., Gilli, G., Grassi, D., Haus, R., Herrmann, M., Imamura, T., Kohler, E., Krause, P., Migliorini, A., Montmessin, F., Pere, C., Persson, M., Piccialli, A., Rengel, M., Rodin, A., Sandor, B., Sornig, M., Svedhem, H., Tellmann, S., Tanga, P., Vandaele, A. C., Widemann, T., Wilson, C. F., Müller-Wodarg, I., and Zasova, L. (2017). The thermal structure of the Venus atmosphere: Intercomparison of Venus Express and ground based observations of vertical temperature and density profiles*. *Icarus*, 294:124–155.

Scarica, P., Garate-Lopez, I., Lebonnois, S., Piccioni, G., Grassi, D., Migliorini, A., and Tellmann, S. (2019). Validation of the IPSL Venus GCM thermal structure with Venus Express data. *Atmosphere*, 10:584.

Soret, L., Gérard, J. C., Montmessin, F., Piccioni, G., Drossart, P., and Bertaux, J. L. (2012). Atomic oxygen on the Venus nightside: Global distribution deduced from airglow mapping. *Icarus*, 217:849–855.